

Hologram Quantitative Structure Activity Relationship Analysis of JNK Antagonists

Seema A. Kulkarni¹ and Thirumurthy Madhavan^{2†}

Abstract

c-Jun N-terminal kinase-3 (JNK3) is a member of the mitogen-activated protein kinase family (MAPK), and plays an important role in neurological disorders. Therefore, identification of selective JNK3 inhibitor may contribute towards neuroprotection therapies. In this work, we performed hologram quantitative structure-activity relationship (HQSAR) on a series of thiophene trisubstituted derivatives. The best predictions were obtained for HQSAR model with $q^2 = 0.628$ and $r^2 = 0.986$. Statistical parameters from the generated QSAR models indicated the data is well fitted and have high predictive ability. HQSAR result showed that atom, bond and chirality descriptors play an important role in JNK3 activity and also shows that electronegative groups is highly favourable to enhance the biological activity. Our results could be useful to design novel and selective JNK3 inhibitors.

Keywords: JNK, HQSAR

1. Introduction

The c-Jun N-terminal kinases (JNKs) are a family of serine/threonine protein kinases of the mitogen activated protein kinase (MAPK). It activates various transcription factors such as c-jun by phosphorylation of serine/threonine residues^[1-3]. However ongoing studies indicate that JNKs can phosphorylate a variety of additional transcription factors such as ATF-2, Elk-1, NFAT and p53. Furthermore, JNKs can play a wider intracellular role through their phosphorylation of non-nuclear proteins. For example, an important role for the JNKs has been suggested in the regulation of apoptosis. In mammals, there are three JNK genes (*jnk1*, *jnk2* and *jnk3*), each on a different chromosome^[4]. JNK1 and JNK2 are ubiquitously expressed while JNK3 is localized primarily in brain. JNK3 has been implicated in playing important roles in models of neurodegeneration such as the synaptic loss associated with Alzheimer's

disease, mediation of neurotoxicity in Parkinson's disease as well as involvement in Huntington's disease and cerebral ischemia. For a JNK3 inhibitor to demonstrate in vivo neuroprotection it must be brain penetrant and have high kinase selectivity to avoid potential toxicity^[5].

The X-ray crystal structures of all three JNK isoforms have been reported. The overall architecture of JNKs is highly similar to that of other MAP kinases such as ERK2 and p38^[6,7]. The amino acid sequence identity of the JNK kinases is higher than 90%, with over 98% homology within the ATP binding site. The high homology of the ATP binding site within JNK's makes it challenging to design isoform-specific ATP-site directed inhibitors. Therefore, designing selective ATP, competitive JNK (1, 2, and 3) inhibitors is still a challenging task. As selectivity is the major issue, our in silico analysis might be the starting point for the synthesis of highly potent and selective JNK3 analogs, and this prompted us to initiate the analysis. The main aim of our study was to optimize the reported selective JNK3 inhibitors using HQSAR method.

2. Experimental Section

2.1. Data Set

In this study, the dataset was selected from reported literature^[1], consisted of 31 molecules belonging to the

¹Department of Biotechnology, Karpaga Vinayaga college of Engineering and Technology, GST Road, Madhuranthagam Tk, Kanchipuram Dist 603308, India

²Department of Bioinformatics, School of Bioengineering, SRM University, SRM Nagar, Kattankulathur, Chennai 603203, India.

†Corresponding author : thirumurthyunom@gmail.com,
thirumurthy.m@ktr.srmuniv.ac.in
(Received : April 22, 2015, Revised : June 17, 2015,
Accepted : June 25, 2015)

Table 1. Structures and biological activities (pIC₅₀) of JNK3 inhibitors

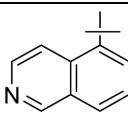
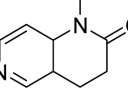
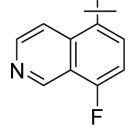
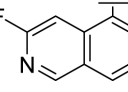
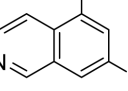
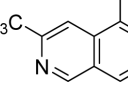
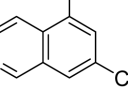
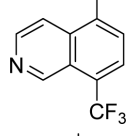
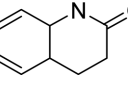
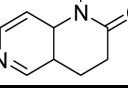
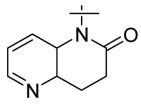
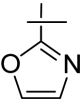
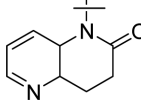
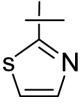
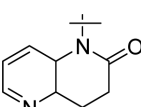
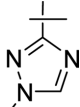
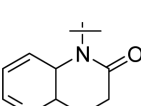
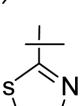
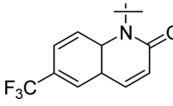
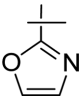
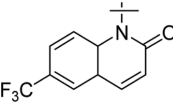
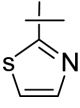
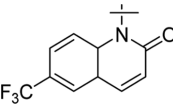
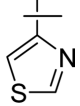
Compound 1-18		Compound 19-24		Compound 25-31	
Compound	R	R1	R2	pIC ₅₀	
1		Cl	-	7.959	
2*		CN	-	8.155	
3		Br	-	7.620	
4*		Br	-	7.523	
5		Br	-	7.387	
6		Br	-	7.284	
7*		Br	-	6.553	
8		Cl	-	6.738	
9		Br	-	7.553	
10		Br	-	7.854	

Table 1. Continued

Compound	R	R1	R2	pIC50
11		CN	-	8.222
12*		Br	-	8.155
13		Br	-	8.222
14		Br	-	7.854
15		Br	-	8.097
16		Br	-	7.854
17*		-	-	8.301
18		-	-	8.046
19		-	-	7.721
20*		-	-	7.149
21		-	-	8.222
22		-	-	7.721
23		-	-	8.699
24*		-	-	8.699

Table 1. Continued

Compound	R	R1	R2	pIC ₅₀
25			Br	8.222
26			Br	7.824
27			Br	8.523
28			CN	7.959
29*			CN	8.097
30*			CN	8.046
31			CN	8.097

*Test set compounds

series of thiophene trisubstituted derivatives. For analysis, the given inhibitory concentration values were changed to minus logarithmic scale value (pIC₅₀), as a dependent variable for QSAR analysis by using the formula $pIC_{50} = -\log(IC_{50})$. It is common to convert the biological activity data into a logarithmic scale, because the resulting model behaves more reasonably and would usually give better linear models. The dataset was randomly partitioned into training and test set molecules by considering range of molecules so that both the training and test sets consist of high, medium and low activity molecules. The training and test set consist of 31 and 8 molecules, respectively. The structures and biological activities of all compounds including both training set and test set molecules is shown in Table 1. Before performing 3D-QSAR studies, all the structures were fully optimized with Gasteiger-Huckel partial charges,

and subsequently docking as well as 3D-QSAR analysis were performed.

2.2. HQSAR Model Calculation

HQSAR is a technique that employs fragment fingerprints as predictive variables of biological activity or other structural related data^[8]. HQSAR does not require a 3D structure of bioactive conformation or molecular alignments. HQSAR model generation deals with the 2D structure directed fragment fingerprints. These molecular fingerprints are broken into strings at fixed intervals as specified by a hologram length (HL) parameter. The HL determines the number of bins in the hologram into which the fragments are hashed. The optimal HQSAR model was derived from screening through the 12 default HL values, which were a set of 12 prime numbers ranging from 53-401. The model development

was performed using the following parameters: atom (A), bond (B), connection (C), chirality (Ch), hydrogen (H) and donor/acceptor (DA). The validity of the model depends on statistical parameters such as r^2 , q^2 by LOO, and standard error^[9].

2.3. HQSAR Validation

The predictive ability of HQSAR model was expressed using the following formula where SD is the sum of squared deviation between the biological activity of the test set and the mean activity of the training set molecules and the PRESS is the sum of squared deviations between predicted and observed activity value for every molecule in the test set^[10].

$$r_{\text{pred}}^2 = (\text{SD}-\text{PRESS})/\text{SD}$$

Once the structural information is encoded into the molecular hologram, HQSAR runs a PLS analysis to derive the HQSAR in which the molecular holograms generated were used as independent variables. The robustness of the model depends on the more challenging r_{pred}^2 from the test set data.

3. Results and Discussion

3.1. HQSAR Statistical Analysis

HQSAR was performed on 31 trisubstituted thiophene derivative using three distinct parameters [fragment size, the hologram length, and the fragment type (fragment distinction)]. Initially, 14 HQSAR models were generated using the different fragment distinction with the fragment size 4–7. The combination of atom, bond and connection, gave the better model ($q^2 = 0.614$, $r^2 = 0.988$, $\text{SEE} = 0.309$) based on the hologram length of 97 with 6 components. The statistical results of the generated models are shown in Table 2.

To further investigate the influence of the length of fragment sizes various model were generated using following sizes: 2–5, 3–6, 4–7, 5–8, 6–9, 7–10, and 8–11. The statistical parameters showed that there is little improvement of statistical values by changing the fragment size. The results indicated that fragment size 3-6 showing the best HQSAR model ($q^2 = 0.628$, $r^2 = 0.986$, $\text{SEE} = 0.303$) based on the hologram length of 353 with 6 components. The HQSAR models for different fragment sizes and the statistical results are summarized in Table 3.

Table 2. HQSAR analyses for various fragment distinctions on the key statistical parameters using default fragment Size (4-7)

Model no	Fragment distinction	Statistical parameters				
		q^2	r^2	SEE	N	HL
1	A/B	0.586	0.921	0.321	4	257
2	A/B/C	0.614	0.988	0.309	6	97
3	A/B/C/H	0.579	0.876	0.304	4	97
4	A/B/C/Ch	0.614	0.988	0.309	6	97
5	A/B/C/H/Ch	0.577	0.877	0.305	4	97
6	A/C/DA	0.443	0.869	0.360	5	97
7	A/B/C/H/DA	0.500	0.881	0.331	4	307
8	A/B/H	0.497	0.967	0.352	6	307
9	A/B/H/DA	0.314	0.426	0.368	2	199
10	A/B/C/DA	0.498	0.912	0.332	4	307
11	A/B/Ch/DA	0.547	0.889	0.315	4	151
12	A/B/H/Ch	0.475	0.921	0.349	5	307
13	A/B/DA	0.314	0.426	0.368	2	199
14	A/B/Ch	0.555	0.912	0.312	4	353

A=atoms; B= bonds; C=connection; H=hydrogen atoms; Ch=chirality; DA=Donor and acceptor; N= number of statistical components; q^2 = cross-validated correlation coefficient; r^2 = non-cross validated correlation coefficient; SEE=standard error of estimate; HL=hologram length.

Table 3. Influence of various fragment size using the best fragment distinction combination (A/B/C)

Model no	Fragment size	Statistical parameters				
		q ²	r ²	SEE	N	HL
15	2-5	0.624	0.930	0.287	4	257
16^a	3-6	0.628	0.986	0.303	6	353
17	4-7	0.614	0.988	0.309	6	97
18	5-8	0.452	0.812	0.329	2	199
19	6-9	0.526	0.860	0.306	2	199
20	7-10	0.477	0.879	0.330	3	199
21	8-11	0.411	0.750	0.341	2	97

N= number of statistical components; q²= cross-validated correlation coefficient; r²= non-cross validated correlation coefficient; SEE=standard error of estimate; HL=hologram length.

^aThe model chosen for HQSAR analysis is highlighted in bold font.

3.2. Validation of HQSAR Model

The predictive ability of the developed HQSAR model was assessed by the test set (nine molecules) predictions, which were excluded during QSAR model generation. The predictive ability of the test set molecule for HQSAR were 0.743. The actual and predicted activities for the training and test set molecules are given in Table 4 and the scatter plot of predicted versus actual activities for the training set and test set is shown in Fig. 1.

3.3. HQSAR Contribution Map Analysis

The HQSAR results gave direct evidence about the individual atomic contributions to the biological activity through the use of different color codes. The contribution of different fragments for the activity of molecules 23, and 27 are displayed in Figure 2a and 2b, respectively. The colors at the red end of the spectrum indicates the poor contributions (red, red orange, and orange), while colors at the green end reflect favorable contributions (yellow, green blue, and green). Atoms

Table 4. Actual, predicted and residual values for the training set and test set of HQSAR model

Compound	Actual pIC ₅₀	HQSAR		Compound	Actual pIC ₅₀	HQSAR	
		Pred	Residual			Pred	Residual
1	7.959	7.887	0.072	17*	8.301	8.330	-0.029
2*	8.155	7.787	0.368	18	8.046	7.956	0.090
3	7.620	7.590	0.030	19	7.721	7.818	-0.097
4*	7.523	7.490	0.033	20*	7.149	7.296	-0.147
5	7.387	7.469	-0.082	21	8.222	8.243	-0.021
6	7.284	7.266	0.018	22	7.721	7.725	-0.004
7*	6.553	6.961	-0.408	23	8.699	8.618	0.081
8	6.738	6.711	0.027	24*	8.699	8.586	0.113
9	7.553	7.533	0.020	25	8.222	8.206	0.016
10	7.854	7.912	-0.058	26	7.824	7.831	-0.007
11	8.222	8.296	-0.074	27	8.523	8.521	0.002
12*	8.155	8.518	-0.363	28	7.959	7.916	0.043
13	8.222	8.191	0.031	29*	8.097	7.976	0.121
14	7.854	7.885	-0.031	30*	8.046	7.637	0.409
15	8.097	8.103	-0.006	31	8.097	8.144	-0.047
16	7.854	7.890	-0.036				

*Test set molecules

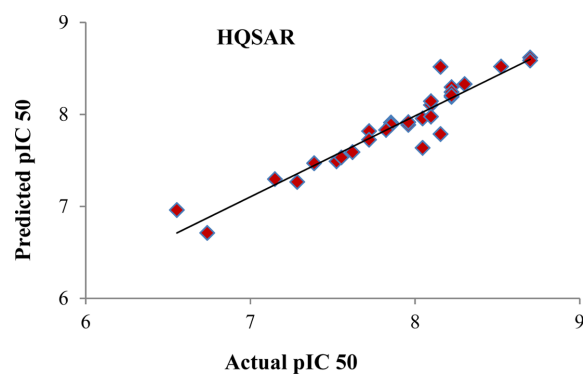


Fig. 1. Scatter plot diagram of predicted versus actual activity of training and test set compounds by HQSAR analysis.

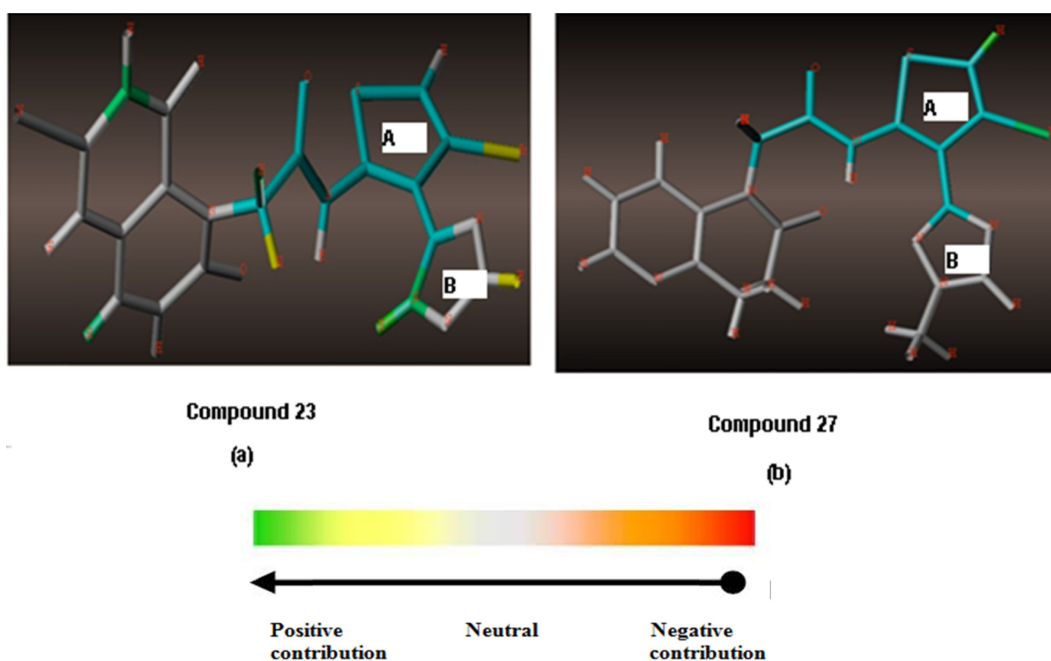


Fig. 2. (a, b): HQSAR contribution map for most active compounds 23 and 27.

with intermediate contributions are colored in white. From Fig. 2 and 2b, fragment contribution map shown that A and B ring scaffold were strongly related to the biological activity of highly active compounds, as it is represented in blue, yellow and white color codes. The generated HQSAR model clearly explained the potent activity of compound 23 and 27. The five member ring of the highly active compounds 23 and 27 contain a bromine and sulphur atoms and are shown in blue and yellow color. Therefore, bromine and sulphur can serve as structural scaffold for holding the pharmacophoric

groups are necessary for activity and it shows that electronegative groups is highly favourable to enhance the biological activity. This fragment may be preferred when designing new scaffold for designing JNK3 inhibitors.

4. Conclusion

In the present work, we have performed HQSAR analysis on a set of trisubstituted thiophene derivatives. The HQSAR model shows the importance of atom,

bond, and connection parameters. The overall study indicates that, in HQSAR analysis, fragments containing information about the ring A and B are important for an inhibitory effect. Our results can be utilized to design more potent compounds than the present series of compounds.

References

- [1] S. Bowers, A. P. Truong, R. J. Neitz, R. K. Hom, J. M. Sealy, G. D. Probst, D. Quincy, B. Peterson, W. Chan, R. A. Galembo Jr., A. W. Konradi, H. L. Sham, G. Tóth, H. Pan, M. Lin, N. Yao, D. R. Artis, H. Zhang, L. Chen, M. Dryer, B. Samant, W. Zmolek, K. Wong, C. Lorentzen, E. Goldbach, G. Tonn, K.P. Quinn, J.-M. Sauer, S. Wright, K. Powell, L. Ruslim, Z. Ren, F. Bard, and T.A. Yednock, "Design and synthesis of brain penetrant selective JNK inhibitors with improved pharmacokinetic properties for the prevention of neurodegeneration", *Bioorg. Med. Chem. Lett.*, Vol. 21, pp. 5521-5527, 2011.
- [2] F. Hilberg, A. Aguzzi, N. Howells, and E.F Wagner, "c-Jun is essential for normal mouse development and hepatogenesis", *Nature*, Vol. 365, pp. 179-181, 1993.
- [3] G. Klebe, "The use of composite crystal-field environments in molecular recognition and the de novo design of protein ligands", *J. Mol. Biol.*, Vol. 237, pp. 212-235, 1994.
- [4] R. Wisdom, R.S Johnson, and C Moore, "c-Jun regulates cell cycle progression and apoptosis by distinct mechanisms", *EMBO J.*, Vol. 18, pp. 188-197, 1999.
- [5] A. Behrens, W. Jochum, M. Sibilía, and E. F Wagner, "Oncogenic transformation by ras and fos is mediated by c-Jun N-terminal phosphorylation", *Oncogene*, Vol. 19, pp. 2657-2663, 2000.
- [6] L. A. Tibbles, Y. L. Ing, F. Kiefer, N. Iscove, J. R. Woodgett, and N. J. Lassam, "MLK-3 activates the SAPK/JNK and p38/RK pathways via SEK1 and MKK3/6", *EMBO J.*, Vol. 15, pp. 7026-7035, 1996.
- [7] D. D. Yang, D. Conze, A. J. Whitmarsh, T. Barrett, R. J. Davis, M. Rincón, and R. A. Flavell, "Differentiation of CD4+ cells to Th1 cells requires MAP kinase JNK2", *Immunity*, Vol. 9, pp. 575-585, 1998.
- [8] C. G. Gadhe, T. Madhavan, G. Kothandan, and S. J. Cho, "In Silico quantitative structure-activity relationship studies on P-gp modulators of tetrahydroisoquinoline-ethyl-phenylamine series", *BMC Struct. Biol.*, Vol. 11, 2011.
- [9] T. Madhavan, J. Y. Chung, G. Kothandan, C. G. Gadhe, and S. J. Cho, "3D-QSAR studies of JNK1 inhibitors utilizing various alignment methods", *Chem. Biol. Drug. Des.*, Vol. 79, pp.53-67, 2012.
- [10] R. D. Cramer, D. E. Patterson, and J. Bunce, "Comparative molecular field analysis (CoMFA). 1. Effect of shape on binding of steroids to carrier proteins", *J. Am. Chem. Soc.*, Vol. 110, pp. 5959-5967, 1988.